Formic acid and Methanol Electro-oxidation and Counter Hydrogen Production Using Nano High Entropy Catalyst

Nirmal Kumar Katiyar[†1], Subramanian Nellaiappan[†2], Ritesh Kumar[†4], Kirtiman Deo Malviya[5], K. G. Pradeep[6], Abhishek K. Singh*[4], Sudhanshu Sharma*[2], Chandra Sekhar Tiwary*[,3], Krishanu Biswas*[1]

[1]Department of Materials Science and Engineering, Indian Institute of Technology Kanpur, Kanpur INDIA, 208016

[2]Department of Chemistry, Indian Institute of Technology Gandhinagar, Gandhinagar - 382355, INDIA

[3]Metallurgical and materials Engineering, Indian Institute of Technology Kharagpur, Kharagpur-382355, INDIA

[4]Materials research center, Indian Institute of Science, Bangalore-560012, INDIA

[5]Department of Materials Engineering, Indian Institute of Science, Bangalore-560012, INDIA

[6]Department of Materials Science and Metallurgical Engineering, Indian Institute of Technology Madras, Chennai-600036, INDIA

† **equal contribution**

Abstract

Renewable harvesting of clean energy using the benefits of multi-metallic catalytic materials of high entropy alloy (HEA, equimolar Cu-Ag-Au-Pt-Pd) from formic acid with minimum energy input has been achieved in the present investigation. The synergistic effect of pristine elements in the multi-metallic HEA drives the electro-oxidation reaction towards non-carbonaceous pathway. The atomistic based simulation based on DFT rationalize the distinct lowering of the d-band center for the individual atoms in the HEA as compared to the pristine counterparts. Further this catalytic activity of the HEA has also been extended to methanol electro-oxidation to show the unique capability of the novel catalyst. The nanostructured HEA, prepared using a combination of casting and cryomilling techniques can further be utilized as the fuel cell anode in the direct formic acid/methanol fuel cells (DFFE).

Keywords: *Hydrogen energy; High entropy alloy; electro-oxidation; DFT; Microscopy.*

1 Introduction

The multi-principal multicomponent alloys, popularly known as High Entropy Alloys (HEAs), containing five or more number of elements (equimolar or closely-equimolar ratio) have heralded a new area of materials design. It opens up vast compositional space and provides access to unique functional properties. The mixing of different elements has widely been utilized as an effective means to improve various properties, especially physical, chemical and electronic[1-3]. High entropy of mixing stabilizes the HEAs in the simple crystal structure (FCC, BCC structure), and provides the inherent structural stability and the flexibility to tune the composition with the desired catalytic entities. This flexibility has enthused us to design and explore these materials for heterogeneous catalysis. The electro-oxidation of formic acid is imperative for the development of direct formic acid fuel cells (DFAFC). Platinum (Pt) and palladium (Pd) are two widely used noble-metal electrocatalysts utilized for catalyzing the formic acid into CO_2 and H_2 for DFAFC [4-6]. There are two competing pathways for this catalytic electro-oxidation process, one of them is direct oxidation, and the other one is indirect oxidation via CO intermediate. Direct oxidation is highly looked for, but it is very difficult for any catalyst to match the high catalytic efficiency of Pt and Pd. Even though the efficiencies of Pt and Pd is high but it is not high enough for the industrial application. To improve the catalytic activity, strategies such as alloying of Pt by less reactive noble metals M (M= Cu, Ag, Au, Ru, etc.) has widely been adopted. Another approach is to engineer the shape of the catalyst to maximize the exposure of the chemically active facets[7, 8]. Recent research focuses on single atom catalysis as a new frontier in the area of heterogeneous catalysis. These catalysts are highly active and stable during reactions[9, 10]. The bonding tendency between the anchoring sites on the support and single metal atoms are the major causes[10] for the unusual activity and stability. However, these catalysts always need substantial the energy input (electrochemical potential) to catalyze the reaction.

In current work, five catalytically active metals; Cu, Ag, Au, Pt, and Pd are mixed in an equimolar ratio to develop a high entropy alloy (HEA) (Figure 1a). The HEAs are prepared using a scalable strategy involving a combination of vacuum-melting followed by low-temperature grinding. In the controlled composition HEAs, the homogeneously mixed solid solution of these elements consists of a 'single atom catalyst' of Pt, stabilized by other elements. These HEAs are utilized for the formic acid electrooxidation, an alternative proposition to generate hydrogen in the counter reaction. Unlike conventional Pt nanoparticles, the HEAs have also been observed to produce a significant amount of CO_2 and hydrogen instantly at zero bias (i.e. without energy input) confirming the spontaneous oxidation of formate ion at anode (HEA) catalyst. Additionally, HEAs have also been explored for methanol electrooxidation. To rationalize the high activity of HEAs from atomistic level, density functional theory (DFT) is used, which establishes the superior performance of HEAs, compared to the pristine transition metals.

2 Materials and Methods

The elements granules (Cu, Ag, Au, Pt, Pd) were purchased from Alfa Aesar, USA, with the purity 99.95 at% and used for preparation of high entropy alloys (Cu-Ag-Au-Pt-Pd) ingot. This was prepared in the high purity argon atmosphere utilizing arc melting. Further, ingot was homogenized at 1000^{o}C for 12 hours to acquire large grains and strong chemical homogeneity. These ingots were pulverized in a liquid nitrogen cooled (at-160±10 ^{o}C) cryomill[11] consisting of 5 cm diameter single ball (tungsten carbide). The extra precautions have been taken during milling by purging argon (Ar) gas, which further protects the powder from oxidation. After six hours of cryomilling, the HEAs-NPs (cryomilled powder) were collected for characterizations.

The morphology, size of the HEA nanoparticles have been characterized using Transmission electron microscope (FEI TITAN and Technai G^2, UT 20 operated at 300 and 200 kV respectively). The chemical composition of the nanoparticle has been estimated using energy dispersive spectroscopic detectors (known Super EDS) attached to TITAN. The elemental mapping signifying distribution of elements in the nanoparticles was obtained using Super EDS detectors. Atomic scale distribution of atoms in the alloy was obtained using three-dimensional atom probe tomography in a local electrode atom probe (LEAP 4000X HRTM, Cameca Instruments, France). APT measurement was performed in laser pulsing mode using 30 pJ laser energy at 250 kHz repetition rates, while the tip was maintained at 60 K. The chemical structure determination has been studied using X-ray photoelectron spectroscopy (XPS, PHI5000, Versa Prob II, FEI Inc.). The XPS peaks charge correction has been made using adventitious carbon (284.6 eV) and the spectral peaks deconvolution have been performed using CASA XPS software. Further, the compositions of the as cast ingot and nanoparticles were determine using electron probe micro analyzer (EPMA- JXA-8230; JEOL, Japan).

The conventional three-electrode system (CHI408C electrochemical workstation) has been used for electrochemical studies. The working electrode was made by mixing 100 mg of catalyst and binder (200 μL of 5% Nafion solution). The isopropanol was added to it to make thin slurry, which is deposited on a glassy carbon electrode (GCE). Platinum electrode/wire was used as the counter electrode, and Ag/AgCl electrode was used as the reference electrode. Supporting electrolyte solutions are KNO_3 (0.5 M) for methanol oxidation and K_2SO_4 (0.5 M) for formic acid oxidation reactions. For cyclic voltammetry (CV) experiments, 500 μL of respective analysts were taken and made up to 10 mL using respective supporting electrolytes. An air-tight electrochemical cell was used for the product formation and analysis. For gaseous products analysis, a gas-tight syringe (1

mL) was used to transfer the evolved gases into gas chromatograph (GC: CIC Baroda) using a TCD (thermal conductivity detector) for detecting H_2 and FID (flame ionization detectors) for detecting CO and CO_2. A standard gas mixture was used for calibrating the GC.

2.1 Computational Methodology

First principles calculations were performed using density functional theory (DFT) as implemented in the Vienna ab-initio simulation (VASP 5.4.1) package[12]. The electronic exchange and correlations were approximated by Perdew-Burke-Ernzerhof (PBE) under generalized gradient approximation (GGA)[13]. The optimization of all structures was performed using a conjugate gradient scheme until the convergence criteria for energies and the forces reached 10^{-5} eV and 0.01 eV Å-1, respectively. All (111) surfaces of Pt, Pd, Ag, Au and Cu were generated from their optimized bulk structures using Virtual NanoLab version 2016.2. The structure had 3 layers of atoms with the bottom two layers frozen, allowing only the topmost layer to relax, to mimic the bulk behavior.

3 Results and discussion

Figure 1b shows XRD (X-ray diffraction) pattern of HEAs, exhibiting a single phase (FCC, a = 0.8173 nm). No peak related to individual elements (i.e., Pt, Pd, Cu, Ag, and Au) is observed in the pattern, confirming alloying of these constituents (detailed XRD analysis is discussed in supplementary information Figure S1). Further, these nanoparticles have been characterized using UV–visible spectroscopy to confirm the nature of nanoparticles. The UV-vis spectrum (Figure 1c) reveals the presence of two distinct and strong SPR bands at λ_{max} = 213 and 224 nm for HEAs. The peak positions are distinctly different as compared to individual peaks of Pt, Pd, Au, Ag and Cu nanoparticles, which is consistent with XRD observation. The digital picture of a colloidal solution of HEAs in methanol is shown as inset of Figure 1c. It is also evident that the HEAs

nanoparticles were easily dispersible in the organic solvent. Figure 1d shows scanning electron micrograph in BSE mode of the melted HEAs, revealing dendritic morphology with uniform chemical composition. The elemental mapping (energy dispersive spectroscopy) using SEM is shown in Figure 1d, revealing homogeneously distribution of the elements. The XPS spectra of the HEAs are shown in Figure 1e. The Pt(4f) core level shows two peaks at 71.1 ($Pt4f_{7/2}$) and 74.4 ($Pt4f_{5/2}$) eV similar to bulk Pt[14]. Au(4f) core level spectra show two peaks at 84.0 eV and 88.0 eV related to Au($4f_{7/2}$) and Au($4f_{5/2}$) respectively, which is again similar to bulk Au. In the same way binding energy (B.E.) of Pd, Cu confirms the pure metallic characteristic with binding energies similar to its bulk counterpart. Interestingly, in HEAs, the B.E. for $Ag3d_{5/2}$ appears at 367.8 eV, which 0.4 eV lower than metallic Ag. This phenomenon is consistent with the XPS of bimetallic Au-Ag alloy.

The Figure 2a low magnification dark field HAADF (High Angle Annular Dark Field) micrograph of the HEAs covering several nanoparticles, revealing uniform size and composition (supplementary information Figure S2). The inset shows the selected area diffraction pattern of the FCC phase. Figure 2b shows HAADF image of one HEAs nanoparticle and its irregular morphology with a uniform composition contrast. The EDS composition map of the particle reveals uniform composition distribution. The HRSTEM (High resolution scanning transmission electron microscopy) image in HAADF shows Z contrast, revealing the composition of the individual lattice. It clearly shows a homogeneous mixture of constituent elements. The result of the 3D APT analysis is shown in Figure 2d. The elemental distribution for the constituent elements (Ag, Cu, Pt, Pd, and Au) in the specimen is automatically homogeneous, indicating the formation of homogeneous multicomponent alloy in the nanocrystalline form. The detailed composition

analysis using wavelength dispersive spectroscopy (WDS) is discussed in supplementary information Figure S3.

The electrocatalytic performance of HEAs is assessed by the electro-oxidation of methanol (Figure 3a) and formic acid (Figure 3b) in the neutral electrolytes. Neutral electrolyte is used to avoid the possible leaching of copper phase. Cyclic voltammetry (CV), during the methanol oxidation shows the onset oxidation potential at 0.27 V with an intense peak at 0.8 V. This is attributed to the formation and oxidation of CH_3OH[15]. In the reverse (cathodic) scan, a minor anodic peak at 0.42 V appears due to the re-oxidation of methanol preceded by the reduction of the oxidized surface [16]. The ratio of forward peak current (i_f) to reverse peak current (i_r) of HEAs (i_f/i_r =4) is four times higher than the conventional Pt nanoparticles (i_f/i_r =1, supplementary information Figure S4a) indicating that the HEAs catalyst dominantly follows direct oxidation pathways with very less CO formation.

Potentiostatic study (Chronoamperometry) is carried out in an air-tight cell containing methanol (500 µl) and 0.5 M KNO_3 (9.5 ml) at a fixed potential of 0.8V for 1000 sec (supplementary information Figure S4b). Initially, a gradual decrease in current is noticed which reaches a steady state giving a current of 14.7 µA. During the process, enormous amount of hydrogen gas (counter reaction product) is detected other than the products like CO and CO_2. Upon comparing it with conventional Pt nanoparticles (supplementary information Figure S4c), one can notice that the amount of hydrogen is lower than the high entropy alloy catalyst. Also, the amount of free CO is also much lower (~ 4 times) than the Pt nanoparticles confirming the major contribution from direct oxidation pathways on HEA.

In the same way, the catalytic activity on formic acid is also demonstrated (Figure 3b). The onset of oxidation is at 0.0 V with the current value of ~3.5 mA, in contrast to the Pt nanoparticles where

the current is zero at 0.0 V (supplementary information Figure S5a). In the case of HEAs, a well-defined oxidation peak at ~0.69 V with a current value of 4.27 mA is observed, which is related to the oxidation of HCOOH. Similarly, in the reverse scan, an anodic peak at ~0.32 V with a current value of 2.89 mA is observed, which can be assigned to the HCOOH oxidation preceded by the surface reduction [17, 18]. The forward and reverse peak current ratio (i_f/i_r) in the HEAs is 1.47, which is about 3.5 times higher than the conventional Pt nanoparticles (0.4). This confirms the major contribution from the direct oxidation pathway[17-19]. Chronoamperometry at 0.7 V for 1000 seconds on HEA in an air-tight cell is carried out to analyze the evolved gases (Figure 3c). As soon as the potential is applied, a large number of bubbles (image on Figure 3c) form instantaneously over HEAs (working electrode). The gaseous products formed are analyzed using GC. Large amount of hydrogen (counter reaction product) is also detected, which is accompanied by CO_2 and a noticeable amount of CO (supplementary information Figure S5b,c). Detection of the free CO indicates it also has a contribution in the oxidation mechanism other than the adsorbed CO. Similar chronoamperometry experiment (supplementary information Figure S5d) with Pt nanoparticles produces hydrogen with a higher amount of CO_2 and CO (supplementary information Figure S5h,i) as compared to HEAs (Table 1).

The formic acid oxidation even at unbiased 0.0 volts (Figure 3d) has led to the conclusion that the catalyst possibly works under the unbiased (open circuit potential, OCP) condition as well. Therefore, the electro-oxidation under open circuit potential is carried out for 2000 seconds (Figure 3d image). After 2000 seconds, the gaseous products show the signals for hydrogen, CO_2, and CO (supplementary information Figure S5f,g) proving that the HEAs has the ability to oxidize formic acid under zero potential. Under similar OCP condition, Pt nanoparticles (Figure S5e) does not show any detectable hydrogen (supplementary information Figure S5h,i). From Table 1 it is clear

that under all conditions HEAs catalyst outperforms the Pt nanoparticles in regards to carbon dioxide and counter hydrogen production. Importantly, the amount of CO produced in HEAs is comparatively lower than Pt nanoparticles, revealing the dominance of direct oxidation pathway in both methanol and formic acid. Figure 3e-g shows a comparison of gaseous product during the electro-oxidation of methanol (Figure 3e) and formic acid under biased (Figure 3f) and unbiased (Figure 3g) conditions. From this bar diagram, one can deduce the superior activity of HEAs compared to Pt nanoparticles. It is worth mentioning that this is the first observation for the electro-oxidation of formic acid in an unbiased condition and it paves the way to generate hydrogen in an electrolysis cell from formic acid with minimum input of energy and low CO and CO_2 formation. It is worth noticing that in both methanol and formic acid electrooxidation, the carbonaceous products are not in the stoichiometric balance with hydrogen. This is possibly due to some other side reactions causing the undetected liquid products. In literature, the PtRu alloy has been employed to enhance the activity of methanol and formic acid oxidation. It is stated that the presence of Ru enhances the OH adsorption and enhances the oxidation of CO to CO_2 [15]. One can anticipate the similar mechanism may operate in the HEAs as well. However, the role of individual metallic species is experimentally difficult to distinguish and pinpoint.

Based on the above experimental observations, it is difficult to assign the catalytic role of individual constituent's elements in the multi-component HEAs. Therefore, to gain an insight of the process, we have performed DFT calculations. The electro-oxidation of formic acid is chosen as a representative model reaction for the simulation. The catalytic activity of the HEAs is compared with all its pristine components. The optimized lattice parameters of Pt are, a = b = c = 3.92 Å, which is in excellent agreement with previous reports. The most stable (111) facets in FCC metals were chosen for calculations. The same supercell size was used for all the (111) facets of

pristine metals – Pt, Pd, Ag, Au, and Cu as well as for HEAs. Special quasirandom structure (SQS) of the Cu-Ag-Au-Pt-Pd alloy (HEA) was generated from 5x3x1 supercell of Pt (111) surface using the "mcqs" code employed in Alloy Theoretic Automated Toolkit (ATAT)[20], which is shown in supplementary information Figure S6. The quasirandom structures are generated in ATAT through a Monte Carlo simulated annealing method using an objective function that perfectly matches the maximum number of correlation functions[20]. Such SQS can mimic the thermodynamic and electronic properties of actual structures to a reasonable extent, as has been exemplified in the earlier reports[21, 22]. The unit cell of the HEA-SQS contained 120 atoms, with the Pt, Pd, Ag, Au and Cu atoms comprising 20% each in the total composition. To make an estimate of the activity of HEA and the pristine metal surfaces, their d-band centers were calculated, as they are important descriptors of the catalytic activity. The activity of formic acid decomposition has also been found related to the d-band center of the metal under consideration[19]. The experimentally observed increase in activity of HEA can be explained from Figure 4, where the d-band centers of HEA have been compared with all pristine metal (111) surfaces. The d-band centers of all components except Au (in which d-band centers remain the same) become closer to the fermi-level, leading to the increase in activity.

Subsequently, the formic acid (HCOOH) decomposition was performed on pristine Pt (111) and HEA surface. The adsorption of the key intermediate (formate (HCOO*)) along with the reactant (HCOOH) and product (CO_2) on both surfaces were performed. These adsorption energies were calculated according to the given expressions:

$$\Delta E_{ads}^{HCOOH} = E_{HCOOH}^{*} - (E^{*} + E^{HCOOH}) \quad (1)$$

$$\Delta E_{ads}^{HCOO} = E_{HCOO}^{*} - (E^{*} + E^{HCOOH} - {}^{1}/_{2}\, E^{H_2}) \quad (2)$$

$$\Delta E_{ads}^{CO_2} = E_{CO_2}^{*} - (E^{*} + E^{CO_2}) \quad (3)$$

where, * represents the catalyst surface. Only Pt and Pd atoms were chosen as catalytic sites for the case of HEA, as they were found to be most active among all five metals from the d-band center analysis (Figure 4a). The proposed mechanism has been shown in Figure 4b, and discussed in the caption. The reaction profile for formic acid decomposition on Pt (111) surface is endothermic, while that on HEA surface is exothermic, rendering this reaction more facile on the HEA surface (Figure 4c). Moreover, the adsorption energy of formate intermediate is more negative on Pt (111) surface, leading to lesser residence time of formate on the HEA surface. These two reasons could be ascribed for experimentally higher observed activity of HEA, compared to the pristine Pt catalyst. The evolution of CO_2 gas does not proceed through bent CO_2 intermediate, as this hypothetical structure gets relaxed to the linear CO_2 molecule (supplementary information Figure S7). Therefore, it confirms the mechanism provided in Figure 4b, where hydrogen removal and O-M (M = metal atom of the catalyst) bond scission takes place at the same time. While the two oxygen atoms in CO_2 molecule is equidistant from the Pt (111) surface, it is tilted towards Pd atom on HEA catalyst. This gives an indication of difference in the mechanism of formic acid decomposition on the two surfaces, as the Pd-O bond dissociation might have been followed by Pt-O bond on HEA surface.

Based on experimental and theoretical understanding, we attribute the superior catalytic performance of HEAs (Cu-Ag-Au-Pt-Pd alloy) to the synergism between the metals, i.e. cocktail effect. The remarkable electrocatalytic activity of HEAs in unbiased condition (zero potential) and apparent surface poisoning tolerance towards carbonaceous species are superior to the Pt nanoparticles. Instantaneous production of high amount of hydrogen at unbiased condition makes HEAs an active catalyst for hydrogen production from formic acid.

4 Conclusion

In conclusion, we demonstrated an easily scalable processing technique to produce compositionally controlled nanocrystalline equiatomic Cu-Ag-Au-Pd-Pt, HEAs. The macroscopic and microscopic techniques have been utilized to reveal the atomic distribution in the homogenous mixed HEAs. The synergistic effect of individual metallic component results in higher catalytic activity towards formic acid and methanol electro-oxidation. The unique instant catalytic activity is shown by dissociating formic acid into CO_2 and hydrogen under zero biased (zero energy input) condition. The amount of carbonaceous gases is surprisingly low with HEAs proving the preferred direct oxidation pathway with the possibility of additional liquid products. The density functional theory (DFT) study establishes the HEAs as a superior catalyst, compared to the pristine transition metals, based on adsorption energies. It also gives a clue of difference in the mechanism of formic acid electro-oxidation on HEAs surface with respect to the pristine Pt. The current findings are extended to methanol electro-oxidation, where a similar high activity is attained. This can further be utilized to develop direct formic acid/methanol fuel cells (DFFC) for green energy generation also harnessing hydrogen from these fuels in an electrolysis cell.

Acknowledgments: Author would like to thanks Department of Science and Technology India. S.S. acknowledges DST-SERB (EMR/2016/000806) project for the funding. R.K. and A.K.S. acknowledge Materials Research Centre, Solid State and Structural Chemistry Unit, and Supercomputer Education and Research Centre for providing the computing facilities.

References:

[1] D.B. Miracle, O.N. Senkov, A critical review of high entropy alloys and related concepts, Acta Materialia, 122 (2017) 448-511, https://doi.org/10.1016/j.actamat.2016.08.081.

[2] Y.F. Ye, Q. Wang, J. Lu, C.T. Liu, Y. Yang, High-entropy alloy: challenges and prospects, Mater. Today, 19 (2016) 349-362, https://doi.org/10.1016/j.mattod.2015.11.026.

[3] B. Gludovatz, A. Hohenwarter, D. Catoor, E.H. Chang, E.P. George, R.O. Ritchie, A fracture-resistant high-entropy alloy for cryogenic applications, Science, 345 (2014) 1153-1158, https://doi.org/10.1126/science.1254581.

[4] M.D. Marcinkowski, J. Liu, C.J. Murphy, M.L. Liriano, N.A. Wasio, F.R. Lucci, M. Flytzani-Stephanopoulos, E.C.H. Sykes, Selective Formic Acid Dehydrogenation on Pt-Cu Single-Atom Alloys, ACS Catalysis, 7 (2017) 413-420, https://doi.org/10.1021/acscatal.6b02772.

[5] Z. Sheng, S. Yuyan, Y. Geping, L. Yuehe, Electrostatic Self-Assembly of a Pt-around-Au Nanocomposite with High Activity towards Formic Acid Oxidation, Angew. Chem. Int. Ed., 49 (2010) 2211-2214, https://doi.org/10.1002/anie.200906987.

[6] R. Iyyamperumal, L. Zhang, G. Henkelman, R.M. Crooks, Efficient Electrocatalytic Oxidation of Formic Acid Using Au@Pt Dendrimer-Encapsulated Nanoparticles, J. Am. Chem. Soc., 135 (2013) 5521-5524, https://doi.org/10.1021/ja4010305.

[7] A.-X. Yin, X.-Q. Min, Y.-W. Zhang, C.-H. Yan, Shape-Selective Synthesis and Facet-Dependent Enhanced Electrocatalytic Activity and Durability of Monodisperse Sub-10 nm Pt–Pd Tetrahedrons and Cubes, J. Am. Chem. Soc., 133 (2011) 3816-3819, https://doi.org/10.1021/ja200329p.

[8] H. Liu, J. Qu, Y. Chen, J. Li, F. Ye, J.Y. Lee, J. Yang, Hollow and Cage-Bell Structured Nanomaterials of Noble Metals, J. Am. Chem. Soc., 134 (2012) 11602-11610, https://doi.org/10.1021/ja302518n.

[9] Z. Chengzhou, F. Shaofang, S. Qiurong, D. Dan, L. Yuehe, Single-Atom Electrocatalysts, Angew. Chem. Int. Ed., 56 (2017) 13944-13960, https://doi.org/10.1002/anie.201703864.

[10] K. Jiwhan, R. Chi-Woo, S.S. Kalyan, Y. Sungeun, B. Junemin, H.J. Woo, L. Hyunjoo, Highly Durable Platinum Single-Atom Alloy Catalyst for Electrochemical Reactions, Adv. Energy Mater., 8 (2018) 1701476, https://doi.org/10.1002/aenm.201701476.

[11] N. Kumar, K. Biswas, Fabrication of novel cryomill for synthesis of high purity metallic nanoparticles, Rev. Sci. Instrum., 86 (2015) 083903-083908, https://doi.org/10.1063/1.4929325.

[12] G. Kresse, J. Hafner, Ab initio molecular dynamics for liquid metals, Physical Review B, 47 (1993) 558-561, https://doi.org/10.1103/PhysRevB.47.558.

[13] J.P. Perdew, K. Burke, M. Ernzerhof, Generalized Gradient Approximation Made Simple, Phys. Rev. Lett., 77 (1996) 3865-3868, https://doi.org/10.1103/PhysRevLett.77.3865.

[14] J.Z. Shyu, K. Otto, Identification of platinum phases on γ-alumina by XPS, Appl. Surf. Sci., 32 (1988) 246-252, https://doi.org/10.1016/0169-4332(88)90085-2.

[15] T. Iwasita, H. Hoster, A. John-Anacker, W.F. Lin, W. Vielstich, Methanol oxidation on PtRu electrodes. Influence of surface structure and Pt-Ru atom distribution, Langmuir, 16 (2000) 522-529, https://doi.org/10.1021/la990594n.

[16] W. Huang, H. Wang, J. Zhou, J. Wang, P.N. Duchesne, D. Muir, P. Zhang, N. Han, F. Zhao, M. Zeng, J. Zhong, C. Jin, Y. Li, S.T. Lee, H. Dai, Highly active and durable methanol oxidation electrocatalyst based on the synergy of platinum-nickel hydroxide-graphene, Nat. Commun., 6 (2015) 10035, https://doi.org/10.1038/ncomms10035.

[17] W. Gao, J.A. Keith, J. Anton, T. Jacob, Theoretical Elucidation of the Competitive Electro-oxidation Mechanisms of Formic Acid on Pt(111), J. Am. Chem. Soc., 132 (2010) 18377-18385, https://doi.org/10.1021/ja1083317.

[18] A. Bisht, P. Zhang, C. Shivakumara, S. Sharma, Pt-Doped and Pt-Supported La1–xSrxCoO3: Comparative Activity of Pt4+ and Pt0 Toward the CO Poisoning Effect in Formic Acid and Methanol Electro-oxidation, J. Phys. Chem. C, 119 (2015) 14126-14134, https://doi.org/10.1021/acs.jpcc.5b01241.

[19] K. Tedsree, T. Li, S. Jones, C.W.A. Chan, K.M.K. Yu, P.A.J. Bagot, E.A. Marquis, G.D.W. Smith, S.C.E. Tsang, Hydrogen production from formic acid-decomposition at room temperature using a Ag-Pd core-shell nanocatalyst, Nat. Nanotechnol., 6 (2011) 302-307, https://doi.org/10.1038/nnano.2011.42.

[20] A. van de Walle, P. Tiwary, M. de Jong, D.L. Olmsted, M. Asta, A. Dick, D. Shin, Y. Wang, L.Q. Chen, Z.K. Liu, Efficient stochastic generation of special quasirandom structures, Calphad, 42 (2013) 13-18, https://doi.org/10.1016/j.calphad.2013.06.006.

[21] K.C. Hass, L.C. Davis, A. Zunger, Electronic structure of random $Al_{0.5}Ga_{0.5}$ As alloys: Test of the ``special-quasirandom-structures" description, Physical Review B, 42 (1990) 3757-3760, https://doi.org/10.1103/PhysRevB.42.3757.

[22] C. Jiang, C.R. Stanek, K.E. Sickafus, B.P. Uberuaga, First-principles prediction of disordering tendencies in pyrochlore oxides, Physical Review B, 79 (2009) 104203, https://doi.org/10.1103/PhysRevB.79.104203.

Figure

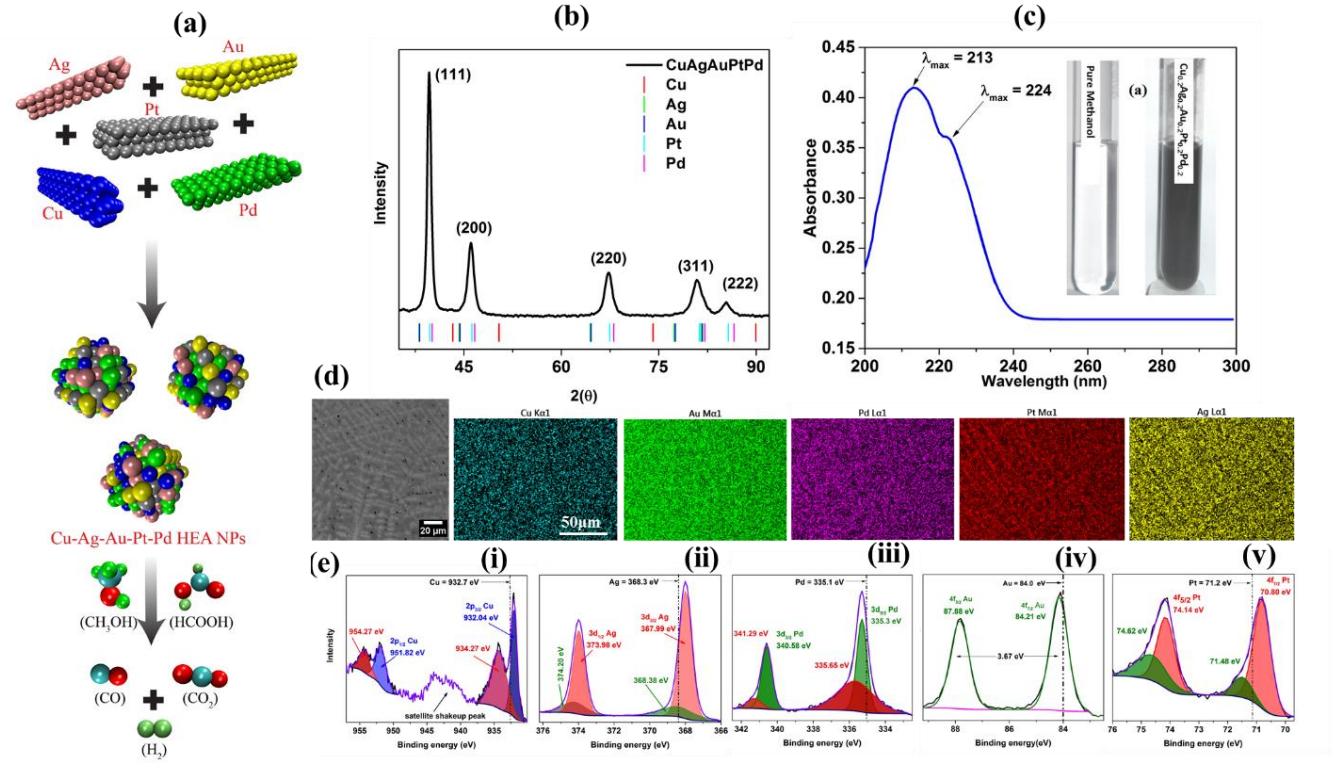

Figure :1 Materials characterization of HEAs: (a) Schematics of HEAs nanoparticle preparation and its activity; (b)X-ray diffraction pattern of HEAs (ingot) as well as nanoparticles (inset shows (111) peak broadening); (c) UV absorbance spectra of nanoparticles dispersed in pure methanol; (d) BSE image of ingot surface (e) SEM-EDAX elemental mapping of ingot surface; (f) X-ray photoelectron spectroscopy spectra of prepared HEAs nanoparticles.

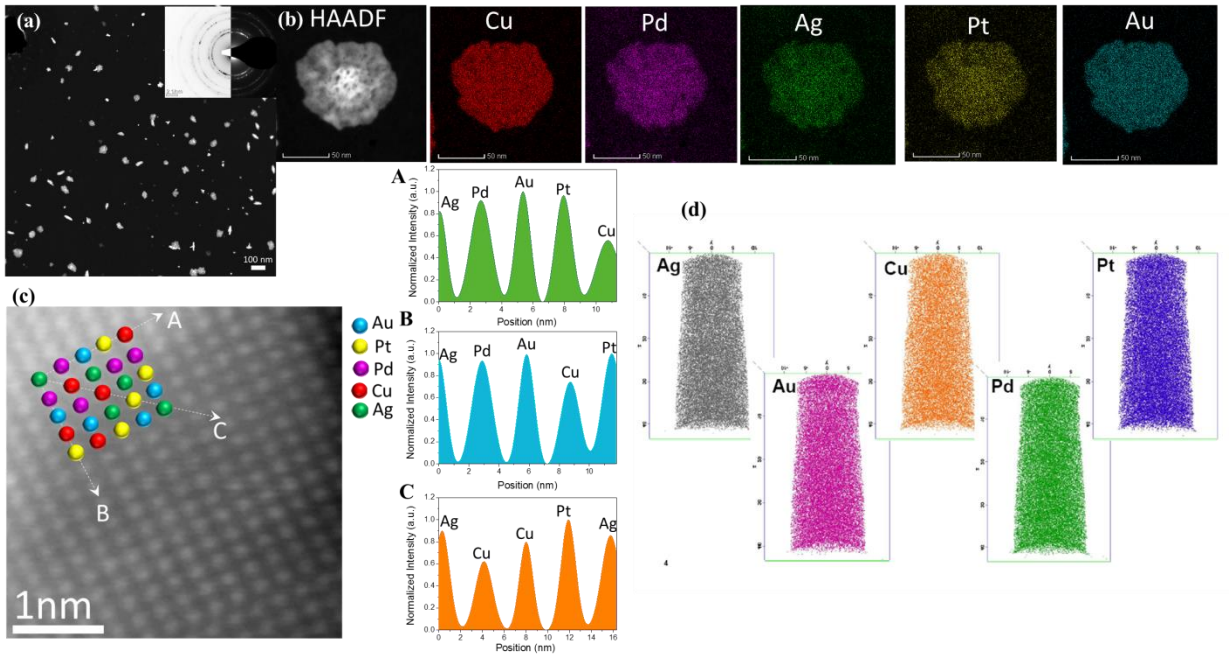

Figure 2: Composition analysis of HEAs: (a)Low magnification darkfield image with large number of particles, inset shows selected area diffraction covering several particles, revealing 111, 200, 220, 311 and 222 reflections. (b) HAADF image of single particle and composition map of the particle. (c) HRSTEM image in HAADF mode of an edge of particle, marked with different intensity (d) elemental distribution of atom probe.

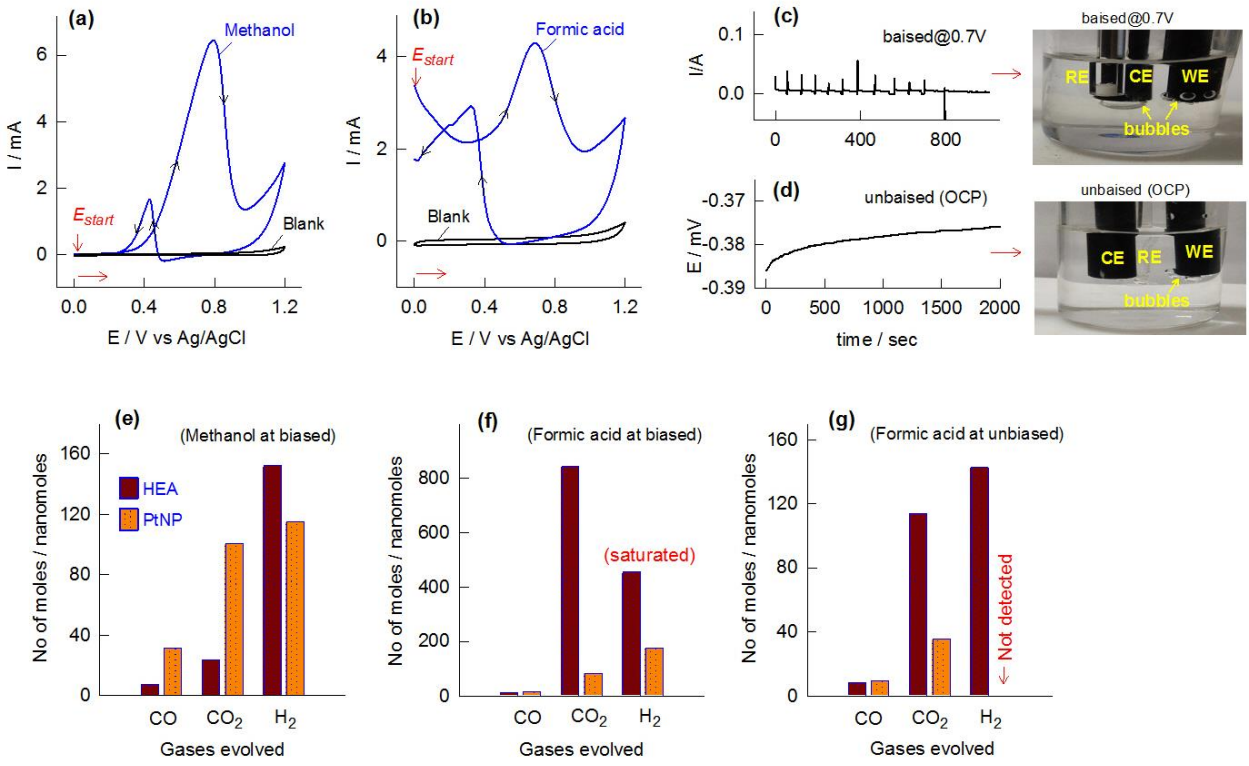

Figure 3: Cyclic voltammetric responses of HEAs deposited glassy carbon electrode for the electro-oxidation of 500 µL methanol in 0.5 M KNO_3 electrolyte **(a)** and 500 µL formic acid in 0.5 M K_2SO_4 electrolyte **(b)** at a scan rate 20 mV s^{-1}. Chrono-amperometric response of HEAs on formic acid at 0.7 V biased for 1000 sec **(c)**, and unbiased (open circuit potential; OCP) for 2000 sec **(d)** in 0.5 M K_2SO_4 electrolyte along with the images taken during their respective experiments. Comparative bar diagrams for the number of moles of gases evolved and detected on HEAs and Pt nano catalyst during methanol oxidation at 0.8 V biased **(e)** and formic acid at 0.7 V biased **(f)** and unbiased OCP **(g)** conditions.

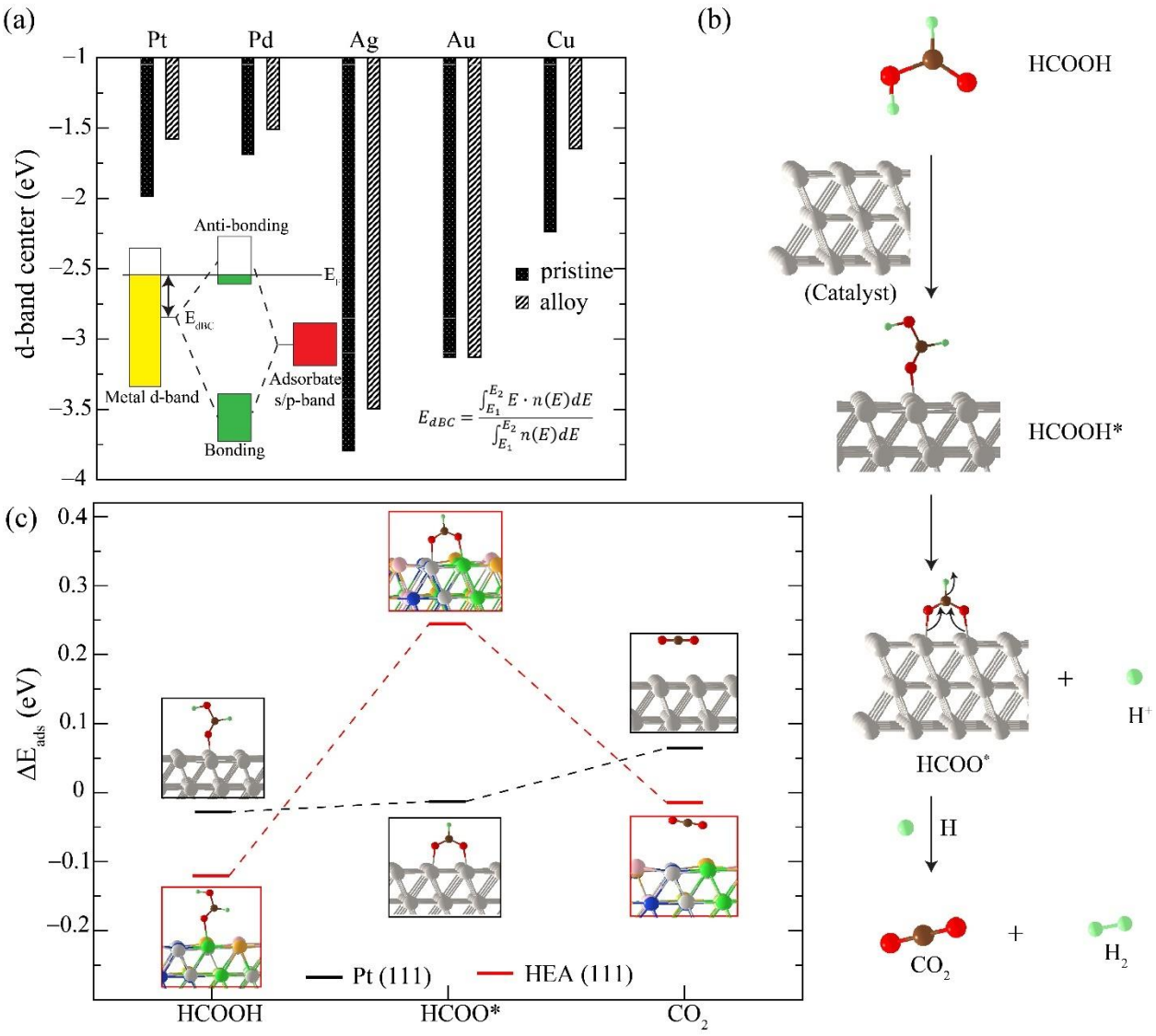

Figure 4: DFT calculation of the hydrogen evolution: ***(a)*** Position of d-band centers (E_{dBC}) of components of alloy Cu-Ag-Au-Pt-Pd, compared with their pristine Pt (111) surfaces' values. E_{dBC} is defined as the first moment of density of d-states (right inset). E and n(E) are the energies and corresponding densities of d-band. E_1 and E_2 are the energy range of d-states. The inset in the left shows how E_{dBC} affects catalytic activity. If E_{dBC} lies closer to the fermi level (E_F), then the antibonding metal-adsorbate state will be filled to lesser extent, thereby stabilizing the metal-adsorbate interactions. ***(b)*** Schematic of formic acid (HCOOH) decomposition on the catalyst surface. At first, HCOOH adsorbs on the catalyst surface through carbonyl oxygen in a monodentate way. Then a proton is released from hydroxyl group, forming a formate intermediate, which adsorbs on the catalyst surface in a bidentate fashion. Finally, CO_2 is released by subsequent removal of another hydrogen attached to carbon, forming H_2 gas a result. ***(c)*** Adsorption energies of reactant, product and the intermediate on pristine Pt (111) (black solid lines) and HEA surfaces (red solid lines) are plotted. The optimized structures of adsorbates on the catalyst surface are shown in black and red insets for Pt (111) and HEA surfaces, respectively. The brown, light green, red, gray, dark green, yellow, blue, and pink spheres represent C, H, O, Pt, Pd, Au, Cu and Ag atoms, respectively in ***(b)*** and ***(c)***.

Table 1: Comparative table for the number of moles of gases evolved and detected (in nanomoles) for the methanol and formic acid catalysis on HEA and Pt nanoparticles catalysts.

Gases detected	HEAs			Pt nanoparticles		
	Methanol	Formic acid		Methanol	Formic acid	
	Biased @ 0.8V	Biased @ 0.7V	Unbiased (OCP)	Biased @ 0.8V	Biased @ 0.7V	Unbiased (OCP)
H_2	152.17	Saturated*	142.61	117.16	176.08	N.D
CO_2	23.95	84.29	113.89	102.56	82.16	35.77
CO	7.58	12.79	8.48	31.63	15.36	9.34

OCP – Open Circuit potential; N.D- not detected; * - Saturated signal

Supplementary Material

Figures S1- X-ray diffraction pattern of HEA ($Cu_{0.2}Ag_{0.2}Au_{0.2}$ $Pt_{0.2}Pd_{0.2}$) ingot and their nanoparticles (NPs) powder prepared by cryo-milling.

Figure 2: (a) Bright field TEM micrograph of Bulk HEA **(b)** corresponding diffraction pattern single particles, **(c)** particles size distribution deduce with nearly 500 particles (nanoparticles TEM bright field shown in main text).

Figure S 3: Electron probe micro analyzer spectra of $Cu_{0.2}$ $Ag_{0.2}Au_{0.2}$ $Pt_{0.2}Pd_{0.2}$ nanoparticles using wavelength dispersive spectroscopy (WDS).

Figure S4. Cyclic voltammetric oxidation response of Pt nanoparticles deposited glassy carbon electrode in methanol (500 μL) at a scan rate 20 mVs^{-1} in 0.5 M KNO_3 electrolyte **(a)**. Chrono-amperometric responses of methanol on HEAs **(b)** and Pt nanoparticles **(c)** deposited glassy carbon electrodes at a fixed potential of 0.8V for 1000 sec in 0.5 M KNO_3 electrolyte along with respective gas chromatography TCD and FID signals.

Figure S5. Cyclic voltammetric responses of Pt nanoparticles deposited glassy carbon electrode for the electro-oxidation of 500 μL formic acid at a scan rate of 20 mV s^{-1} in 0.5 M K_2SO_4 electrolyte **(a)**. Gas chromatograms of both TCD and FID signals for the electro-oxidation of formic acid on HEAs under biased at 0.7 V **(b, c)**. Chronoamperometric response at 0.7 V biased **(d)** and unbiased (OCP) condition **(e)** on Pt nanoparticles in 0.5 M K_2SO_4 electrolyte. Gas chromatograms of both TCD and FID signals for the electro-oxidation of formic acid on HEAs under unbiased (OCP) condition **(f, g)** and on Pt nanoparticles at 0.7V biased **(h)** and unbiased (OCP) condition (i) respectively.

Figure S6. Optimized structures of **(a)** pristine Pt (111) and **(b)** HEA surface as seen from top and side view.

Figure S7. Bent CO_2 intermediate transforms into free linear CO_2 molecule upon relaxation on **(a)** Pt (111) and **(b)** HEA surface.

Table S1: Composition of prepared ingot and nanoparticles, estimated by EPMA-WDS.

Supplementary Material

Formic acid and Methanol Electro-oxidation and Counter Hydrogen Production Using Nano High Entropy Catalyst

Nirmal Kumar Katiyar[†1], Subramanian Nellaiappan[†2], Ritesh Kumar[†4], Kirtiman Deo Malviya[5], K. G. Pradeep[6], Abhishek K. Singh*[4], Sudhanshu Sharma*[2], Chandra Sekhar Tiwary*[,3], Krishanu Biswas*[1]

[1]Department of Materials Science and Engineering, Indian Institute of Technology Kanpur, Kanpur INDIA, 208016

[2]Department of Chemistry, Indian Institute of Technology Gandhinagar, Gandhinagar - 382355, INDIA

[3]Metallurgical and materials Engineering, Indian Institute of Technology Kharagpur, Kharagpur-382355, INDIA

[4]Materials research center, Indian Institute of Science, Bangalore-560012, INDIA

[5]Department of Materials Engineering, Indian Institute of Science, Bangalore-560012, INDIA

[6]Department of Materials Science and Metallurgical Engineering, Indian Institute of Technology Madras, Chennai-600036, INDIA

† equal contribution

1. X-ray diffraction

The XRD analysis has clearly revealed the single phase (FCC) of $Cu_{0.2}Ag_{0.2}Au_{0.2}Pt_{0.2}Pd_{0.2}$ high entropy alloy as shown in **Figure S1**. However, the peak broadening has appeared in case of NPs as shown **Figure S1** (inset peak (111)). Basically, the total broadening is contributed thorough many effects and introduced defects in crystalline order such as instrumental broadening, crystallite size broadening, and micro-strain broadening. Therefore, the major contribution of broadening is due to smaller crystallite size (nanoparticles) and micro-strain (cold working as cryomilling). However, the peaks in the XRD pattern corresponding to the nanoparticles reveal peak broadening (inset showing for (111) peak) indicating nanocrystalline nature. It is to be noted here that the peak broadening is considered to be contributed by instrumental broadening, crystallite size broadening and micro-strain broadening[1]. Therefore, the major contribution of broadening is due to smaller crystallite size (nanoparticles) and micro-strain due to cryommilling.

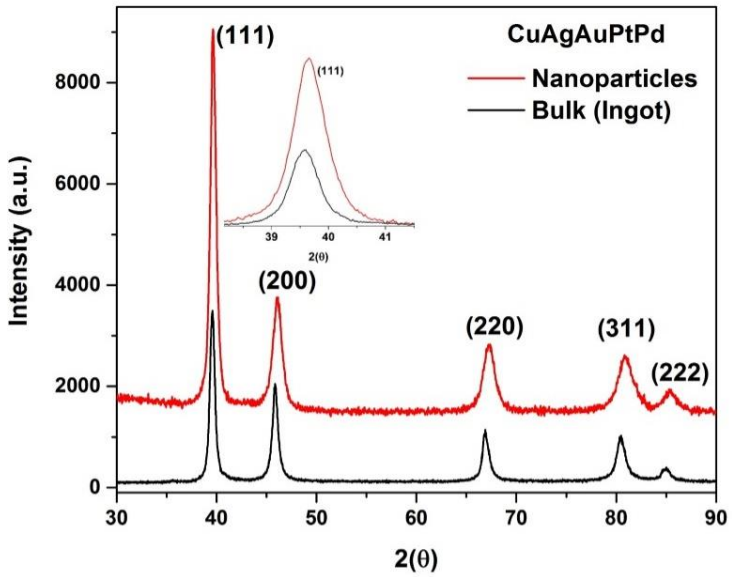

Figure S1: X-ray diffraction pattern of HEA ($Cu_{0.2}Ag_{0.2}Au_{0.2}Pt_{0.2}Pd_{0.2}$) ingot and their nanoparticles (NPs) powder prepared by cryo-milling

2. Transmission Electron Microscope

The **Figure S2a** bright field TEM micrograph of bulk ingot shown, which is clearly evidenced by single phase and the **Figure S2b** shows the FCC diffraction spot pattern. In addition, after 6 hours cryo-milling of the ingot, the size of powder particles has been estimated using TEM as shown in **Figure S2c.** The particles size distributing is 16 ±10 nm as histogram has shown in Figure S2c.

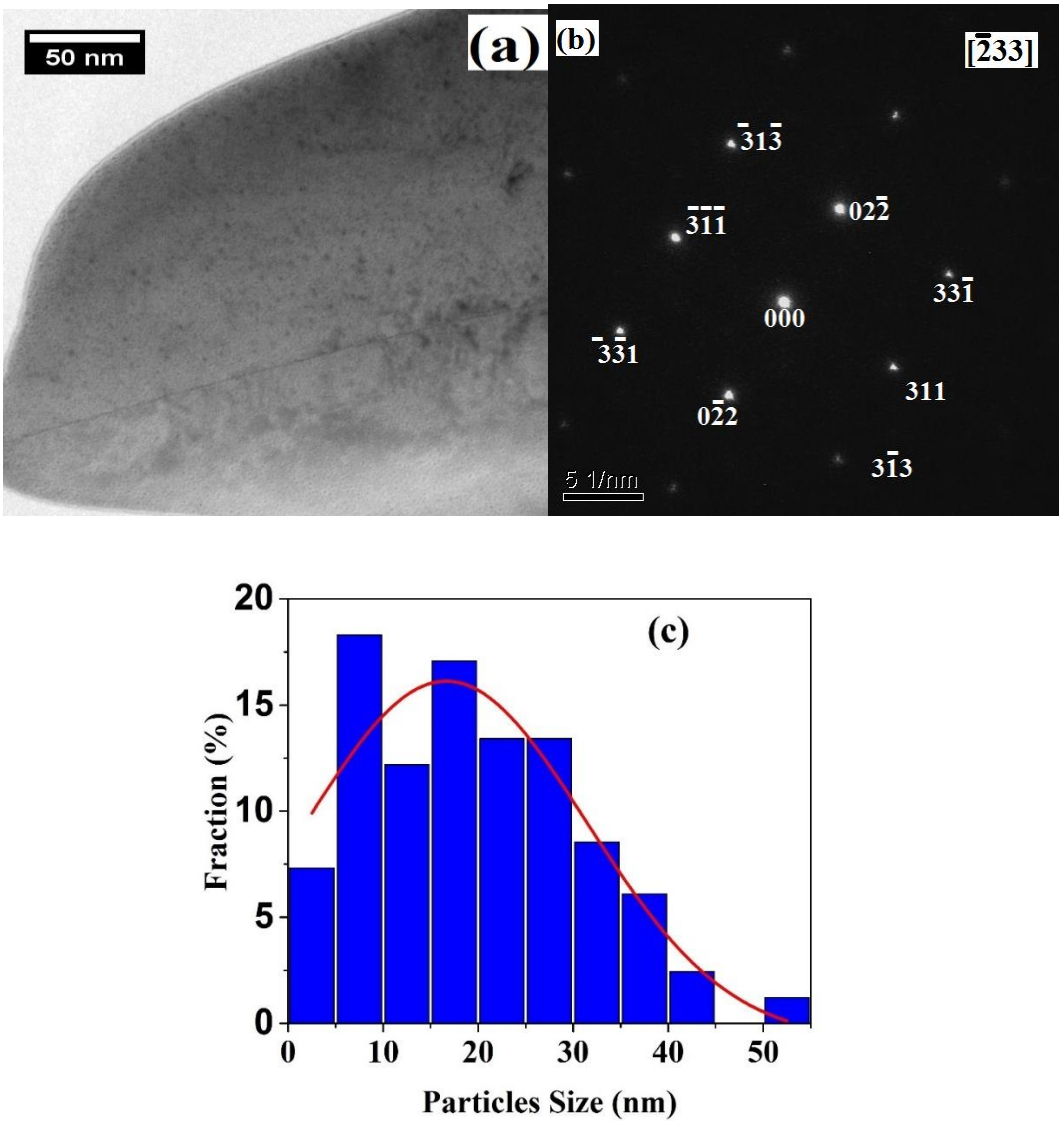

Figure 2:(a) BF-TEM micrograph of as melted HEA **(b)** corresponding diffraction pattern single particles, **(c)** particles size distribution deduce with nearly 500 particles (nanoparticles TEM shown in main text).

3. Composition analysis

The preparation of nanoparticles has a major concern about their purity or foreign contaminations, which arises during the preparation and additives such as capping agents, reducing agent. In case of catalytic activity, the nanoparticles surface play a major role in enhancing their efficiency[2]. Therefore, the used method, cryomilling have the advantage to prepare the clean surface, high purity nanoparticles due to extremely low temperature (protect form oxidation and less contamination from mailing tools due to early grain refinement)[3, 4]The prepared ingot as well as nanoparticles contamination estimated with EPMA-WDS (qualitative and quantitative) as shown in **Figure S3.** There is no contamination have been found except carbon with the detection limit in ideal condition ~10 ppm. The present carbon arises from the carbon tape, which has been used to mount the sample inside a high vacuum chamber. The quantitative composition of prepared ingot and prepared nanoparticles summarized in **Table S1**.

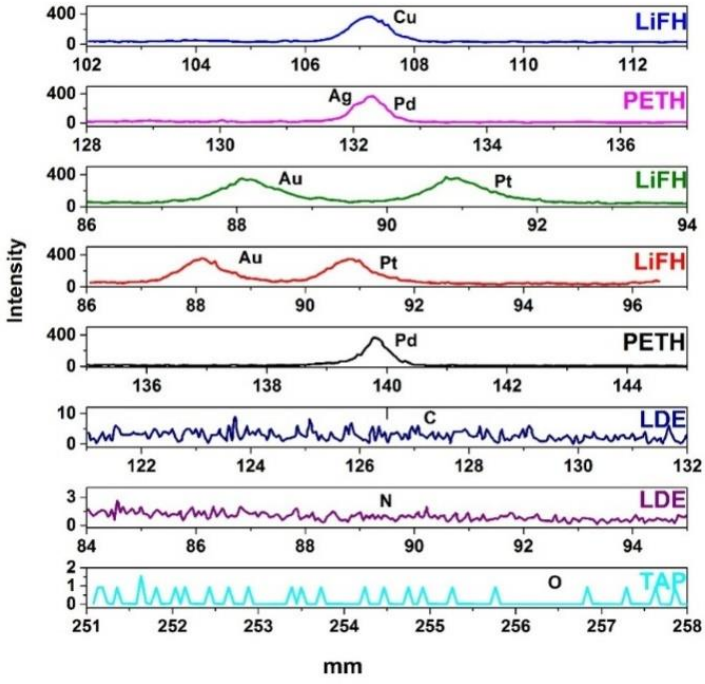

Figure S 3: Electron probe micro analyzer spectra of $Cu_{0.2}Ag_{0.2}Au_{0.2}Pt_{0.2}Pd_{0.2}$ nanoparticles using wavelength dispersive spectroscopy (WDS).

Table S1: Composition of bulk and nanoparticles.

Sample Name	**Composition by wavelength dispersive spectroscopy (WDS) (atom %)**							
	Elements	Pt	Ag	Pd	Cu	Au	O	C

$Cu_{0.2}Ag_{0.2}Au_{0.2}Pt_{0.2}Pd_{0.2}$	Bulk	19.45 ±0.3	20.12 ±0.4	18.34 ±0.3	19.48 ±0.3	20.03 ±0.4	1.48 ±0.2	1.11 ±0.3
	Nano-powder	19.45 ±0.3	18.32 ±0.3	20.50 ±0.3	19.25 ±0.3	20.87 ±0.3	1.01 ±0.3	1.58 ±0.3

Figure S4.

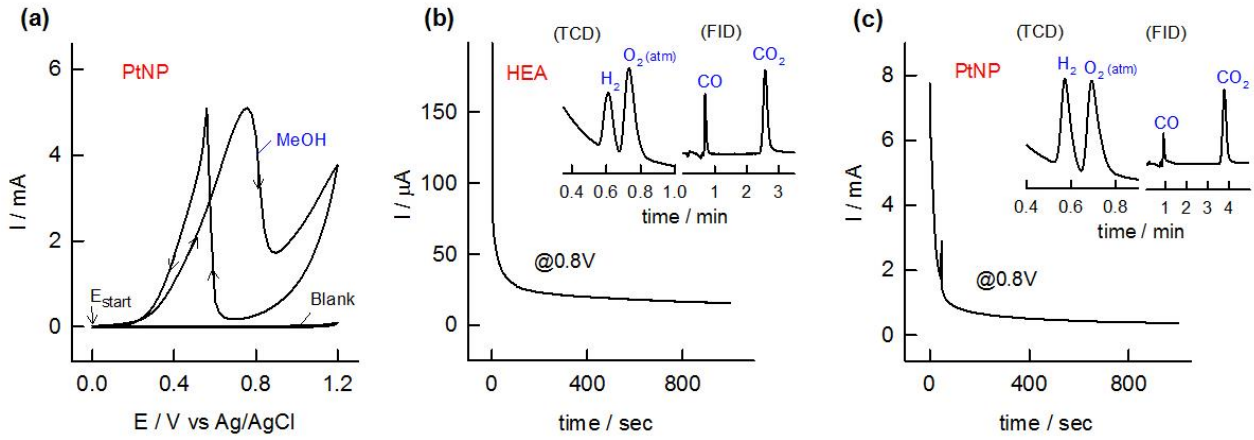

Figure S4. Cyclic voltammetric oxidation response of Pt nanoparticles deposited glassy carbon electrode in methanol (500 µL) at a scan rate 20 mVs^{-1} in 0.5 M KNO_3 electrolyte (a). Chrono-amperometric responses of methanol on HEAs (b) and Pt nanoparticles (c) deposited glassy carbon electrodes at a fixed potential of 0.8V for 1000 sec in 0.5 M KNO_3 electrolyte along with respective gas chromatography TCD and FID signals.

Figure S5.

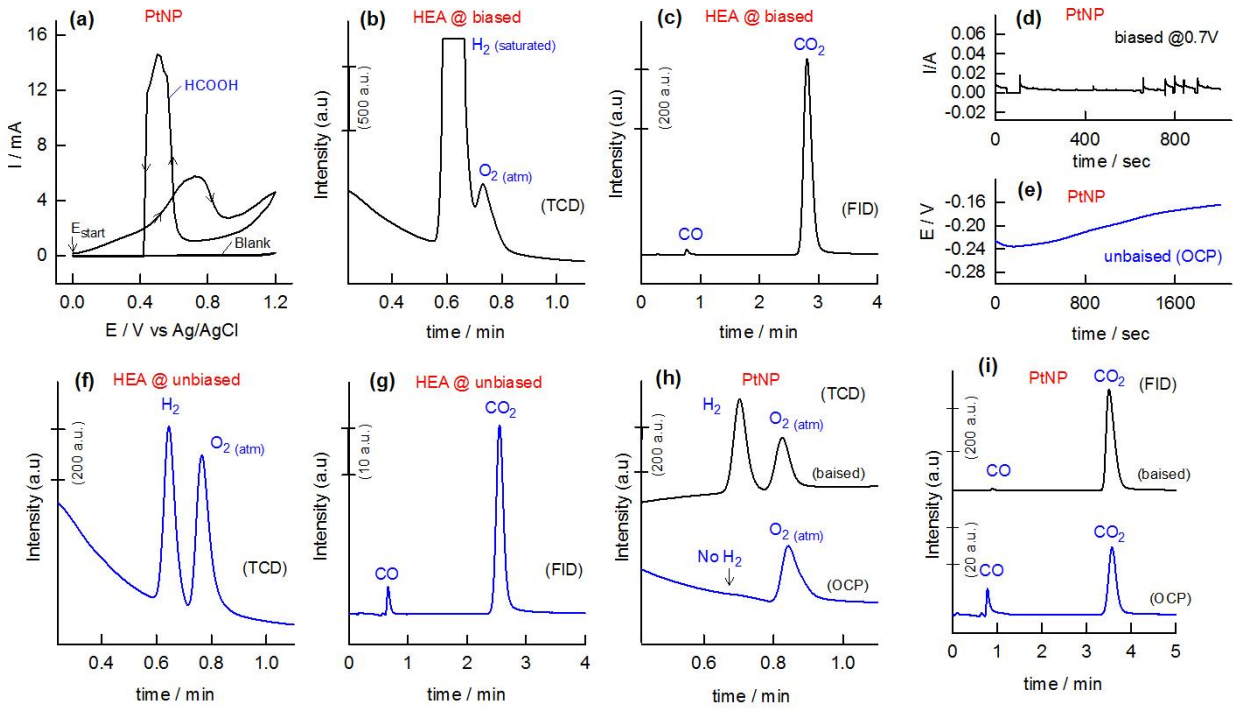

Figure S5. Cyclic voltammetric responses of Pt nanoparticles deposited glassy carbon electrode for the electro-oxidation of 500 µL formic acid at a scan rate of 20 mV s^{-1} in 0.5 M K_2SO_4 electrolyte (a). Gas chromatograms of both TCD and FID signals for the electro-oxidation of formic acid on HEAs under biased at 0.7 V (b,c). Chronoamperometric response at 0.7 V biased (d) and unbiased (OCP) condition (e) on Pt nanoparticles in 0.5 M K_2SO_4 electrolyte. Gas chromatograms of both TCD and FID signals for the electro-oxidation of formic acid on HEAs under unbiased (OCP) condition (f,g) and on Pt nanoparticles at 0.7V biased (h) and unbiased (OCP) condition (i) respectively.

Figure S6.

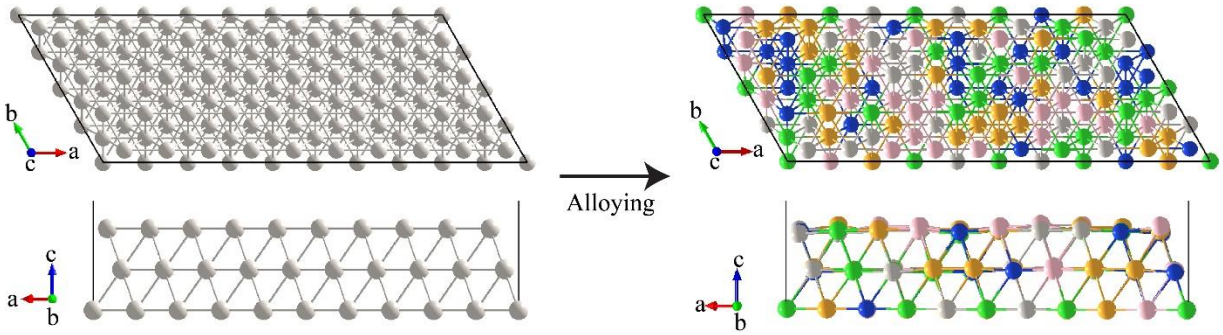

Figure S6. Optimized structures of (a) pristine Pt (111) and (b) HEA surface as seen from top and side view.

Figure S7.

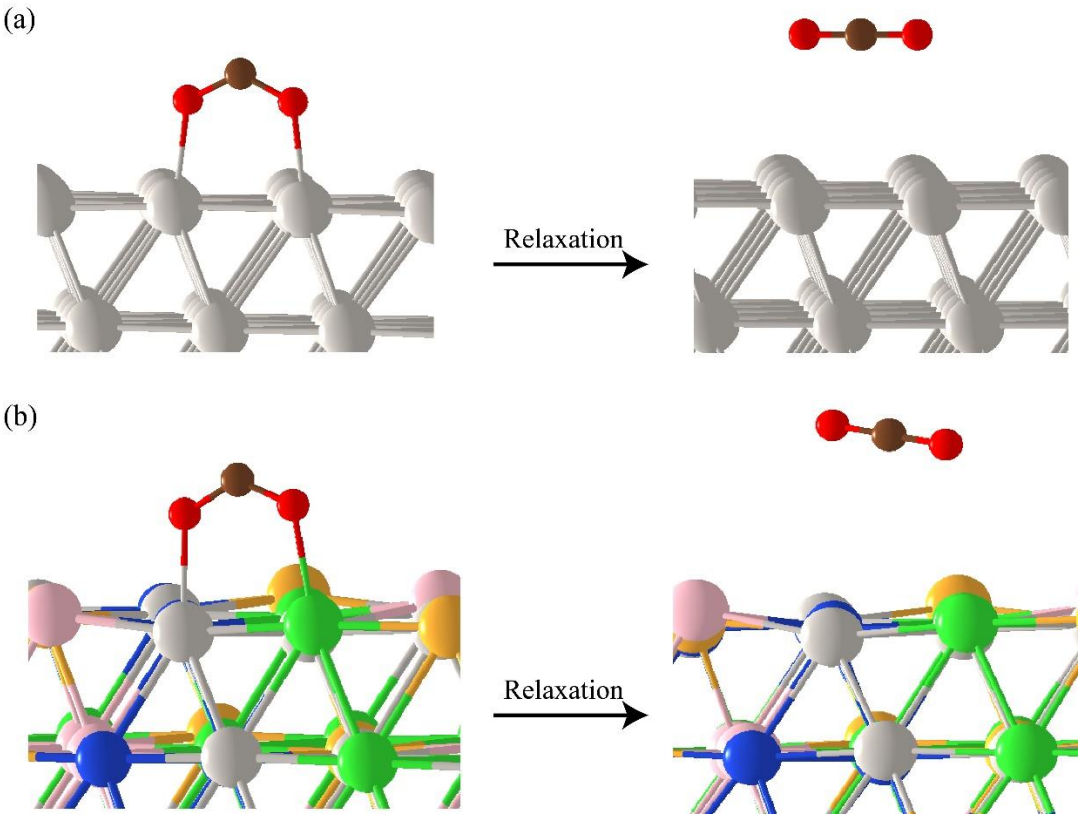

Figure S7. Bent CO_2 intermediate transforms into free linear CO_2 molecule upon relaxation on (a) Pt (111) and (b) HEA surface.

References

[1] G.K. Williamson, W.H. Hall, X-ray line broadening from filed aluminium and wolfram, Acta Metallurgica, 1 (1953) 22-31, https://doi.org/10.1016/0001-6160(53)90006-6.

[2] X. Liu, Y. Sui, X. Yang, Y. Wei, B. Zou, Cu Nanowires with Clean Surfaces: Synthesis and Enhanced Electrocatalytic Activity, ACS Applied Materials & Interfaces, 8 (2016) 26886-26894, https://doi.org/10.1021/acsami.6b09717.

[3] N. Kumar, K. Biswas, R.K. Gupta, Green synthesis of Ag nanoparticles in large quantity by cryomilling, RSC Advances, 6 (2016) 111380-111388, https://doi.org/10.1039/c6ra23120a.

[4] N. Kumar, C.S. Tiwary, K. Biswas, Preparation of nanocrystalline high-entropy alloys via cryomilling of cast ingots, J. mater. Sci., 53 (2018) 13411-13423, https://doi.org/10.1007/s10853-018-2485-z.